

## Supplementary: Numbering-up and sizing-up gliding arc reactors to enhance the plasma-based synthesis of NO<sub>x</sub>

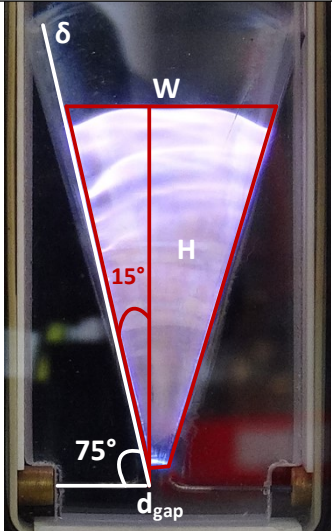
Tijs van Raak<sup>1</sup>, Huub van den Bogaard<sup>1</sup>, Giulia De Felice<sup>1</sup>, Daniël Emmerly<sup>1</sup>, Fausto Gallucci<sup>1,2</sup> & Sirui Li<sup>1\*</sup>

<sup>1</sup> Sustainable Process Engineering, Department of Chemical Engineering and Chemistry, Eindhoven University of Technology, De Rondom 70, Eindhoven, 5612 AP, The Netherlands

<sup>2</sup> Eindhoven Institute for Renewable Energy Systems (EIRES), Eindhoven University of Technology, PO Box 513, Eindhoven, 5600 MB, The Netherlands

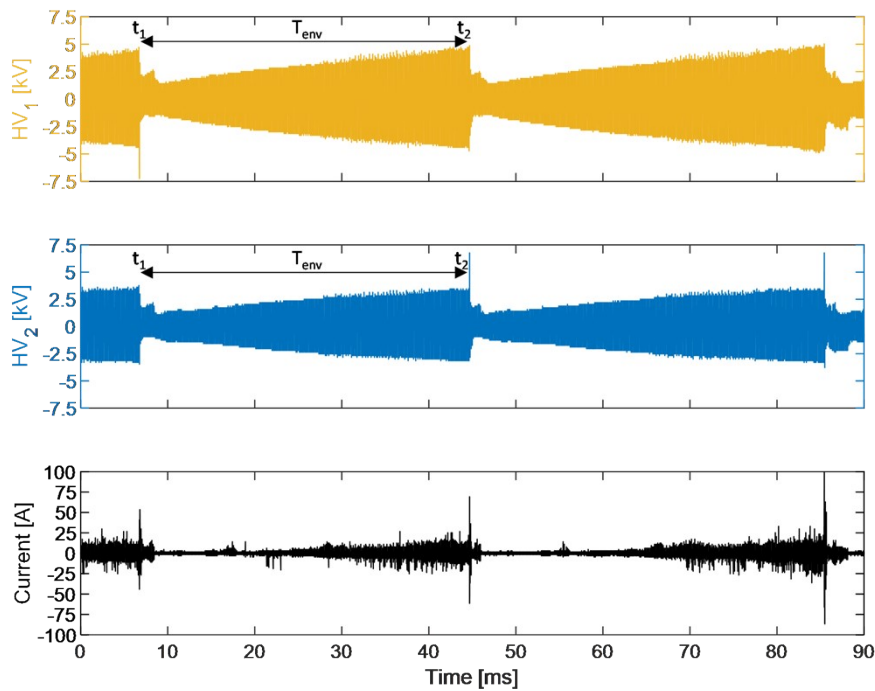
### SI.1. Derivation of the average volume covered by plasma

Figure SI.1 shows a trapezoidal shaped volume predominantly covered by plasma. This figure is an enlarged duplicate of Figure 1 (b) of the main manuscript.  $W$  (mm) was added, which represents the top border of the trapezoid. The general equation of a trapezoid area as function of maximum arc height  $H$  (mm) is shown in equation (S1.1), where  $d_{gap}$  (mm) is the discharge gap at the narrowest point.  $W$  is also a function of maximum arc height and can be calculated with the goniometric tangent function, and the result is represented in equation (S1.2). The electrode angle of 15 degrees was converted in 0.2618 radians. Substituting equation (S1.2) for  $W$  in equation (S1.1), resulted in equation (S1.3), which shows the trapezoid area as function of  $H$  and the constant discharge gap. Multiplying (S1.3) with the electrode thickness  $\delta$  (mm) of 1.00 mm, resulted in the final function to calculate the average plasma volume  $V_{plasma}$ , which is shown in equation (S1.4), and displayed as equation (1) in the main manuscript.

	$Area_{trapezoid}(H) = \frac{1}{2}H(d_{gap} + W)$	(S1.1)
	$W(H) = 2H \tan(0.2618) + d_{gap}$	(S1.2)
	$Area_{trapezoid}(H) = Hd_{gap} + H^2 \tan(0.2618)$	(S1.3)
	$V_{plasma}(H) = d_{gap}H \cdot \delta + \tan(0.2618)H^2 \cdot \delta$	(S1.4)
<p>Figure SI.1: A trapezoidal shaped volume covered by plasma.</p>		

## SI.2. Voltage and current plots for both reactors in series and parallel at various feed flow rates.

Figure SI.2.1 shows the voltages measured across reactor 1 ( $HV_1$ ) & reactor 2 ( $HV_2$ ), and the total supplied current at a feed flow rate of  $1 \text{ L min}^{-1}$  for the system with series-connected reactors. The voltage of the first reactor exceeded the one of the second reactor. The differences between both voltages increased towards the end of every envelope, which explains the differences in supplied discharge power for both reactors. In Figure SI.2.1 a maximum voltage difference of 1.50 kV was measured at the end of both shown envelopes.



**Figure SI.2.1** Voltage and current plots at a  $1 \text{ L min}^{-1}$  feed flow rate for reactors connected in series.

Figures SI.2.2 (a) and (b) show the voltages measured across reactor 1 ( $HV_1$ ) & reactor 2 ( $HV_2$ ), and the total supplied current at a feed flow rate of  $5 \text{ L min}^{-1}$  for the reactors connected in series and parallel, respectively. The envelope times measured in  $HV_1$  are different than the ones in  $HV_2$  for both configurations, which is a result of the circuit complexity as mentioned in the main manuscript. Furthermore, the envelope times for the system with parallel-connected reactors consistently exceeded the ones in series at equal feed flow rates. Moreover, more current peaks were observed for the reactors connected in series, due to increased frequency of arc reignition.

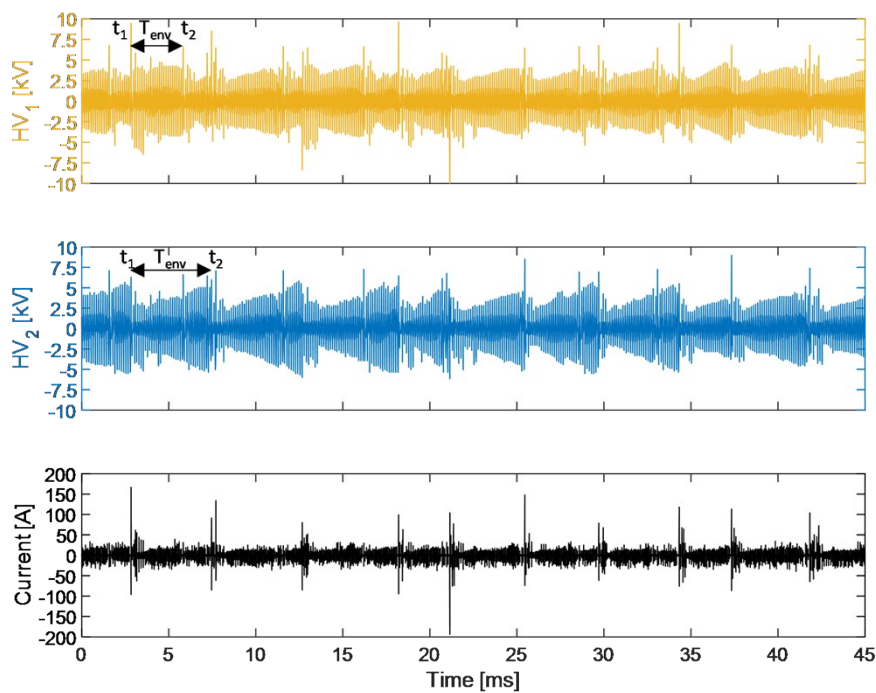


Figure SI.2.2 (a) Voltage and current plots at a 5 L min<sup>-1</sup> feed flow rate for reactors connected in series.

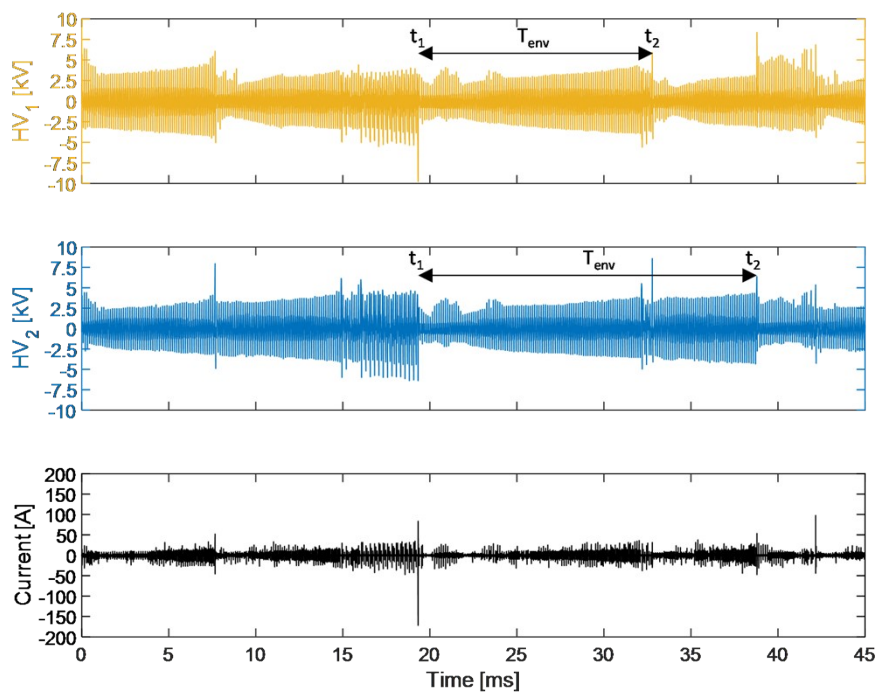


Figure SI.2.2 (b) Voltage and current plots at a 5 L min<sup>-1</sup> feed flow rate for reactors connected in parallel.

### SI. 3. Reduction of the volumetric feed flow rate and calculation of fractional conversions

The molar flow rate can vary significantly, as a result of reactant conversion. The generalized reaction equation (R.S3.1) describes the possible reversible formation of  $NO_x$  in air plasma. Subsequently, the synthesized NO can be oxidized to  $NO_2$  and  $NO_2$  can be dimerized to  $N_2O_4$  as shown in reaction equations (R.S3.2) and (R.S3.3), respectively.

First, atomic nitrogen and oxygen balances were constructed as shown in equations (S3.1) and (S3.2), respectively. The fed compressed dry air (CDA) contained 78 vol%  $N_2$ , 21 vol%  $O_2$ , and 1 vol% of Ar. Ar was considered to be an inert gas. Both equations were summed with the initial molar flow rate of Ar, resulting in the total molar feed flow rate  $F_{T0}$  ( $mmol\ hr^{-1}$ ), as shown in (S3.3).

$N_2 + X O_2 \rightleftharpoons 2 NO_x$	(R.S3.1)
$2 NO + O_2 \rightleftharpoons 2 NO_2$	(R.S3.2)
$2 NO_2 \rightleftharpoons N_2O_4$	(R.S3.3)
$F_{N_{2,0}} = F_{N_2} + 0.5 F_{NO} + 0.5 F_{NO_2} + F_{N_2O_4}$	(S3.1)
$F_{O_{2,0}} = F_{O_2} + 0.5 F_{NO} + F_{NO_2} + 2 F_{N_2O_4}$	(S3.2)
$F_{T0} = F_{N_2} + F_{O_2} + F_{NO} + \frac{3}{2} F_{NO_2} + 3 F_{N_2O_4} + F_{Ar,0}$	(S3.3)

A similar balance was written for the total molar flow rate at the outlet of the reactor  $F_T$  ( $mmol\ hr^{-1}$ ), which is shown in equation (S3.4). Furthermore, the molar flow rate of any specie  $i$  can be rewritten as the volume fraction ( $y_i$ ) of specie  $i$  multiplied by the total molar flow rate as shown in equation (S3.5). The addition of  $0$  was used specifically to indicate the presence in the 'feed'. Rewriting equation (S3.3) as a function of equation (S3.4), and then substituting every  $F_i$  with equation (S3.5) resulted in equation (S3.6). Dividing the total molar flow rate by the total molar feed flow rate resulted in equation (S3.7).

$F_T = F_{N_2} + F_{O_2} + F_{NO} + F_{NO_2} + F_{N_2O_4} + F_{Ar,0}$	(S3.4)
$F_i = y_i F_T$	(S3.5)
$F_{T0} = F_T + 0.5 F_{NO_2} + 2 F_{N_2O_4} = F_T(1 + 0.5 y_{NO_2} + 2 y_{N_2O_4})$	(S3.6)
$\frac{F_T}{F_{T0}} = \frac{1}{1 + 0.5 y_{NO_2} + 2 y_{N_2O_4}}$	(S3.7)

The volumetric feed flow rate was calibrated at a temperature and pressure of 0 °C and 1.013 bar, respectively. Therefore, the total molar feed flow rate is constant and can be calculated using the ideal gas law for every initial feed flow rate. The results are presented in Table S.1.

Table S.1: Molar feed flow rate corresponding to the initial volumetric flow rate.

$F_{v0}$ (L min <sup>-1</sup> )	$F_{T0}$ (mmol hr <sup>-1</sup> )
1.0	2,676.2
1.5	4,014.3
2.0	5,352.5
3.0	8,028.7
4.0	10,704.9
5.0	13,381.1

The total molar flow of reactive nitrogen is defined by equation (S3.8). Combining equations (S3.7) and (S3.8) results in the final molar flow of reactive nitrogen as presented in (S3.9). This flow was used to calculate the EC as shown in equation 7 of the main manuscript.

$F_{N_r} = F_T (y_{NO} + y_{NO_2} + 2 y_{N_2O_4})$	(S3.8)
$F_{N_r} = \frac{F_{T0} (y_{NO} + y_{NO_2} + 2 y_{N_2O_4})}{1 + 0.5 y_{NO_2} + 2 y_{N_2O_4}}$	(S3.9)

Subsequently, the fractional conversion of N<sub>2</sub> was defined in (S3.10) and the one of O<sub>2</sub> in (S3.11). Equations (S3.1) and (S3.2) were substituted in (S3.10) and (S3.11), respectively. The fractional conversions of N<sub>2</sub> and O<sub>2</sub> have been rewritten as a function of total molar flow rates and volume fractions in equations (S3.10) and (S3.11). Substitution of equation (S3.7) in both (S3.10) and (S3.11), resulted in the final expressions for the fractional conversions of N<sub>2</sub> and O<sub>2</sub> as a function of the measured volume fractions of NO, NO<sub>2</sub> and N<sub>2</sub>O<sub>4</sub> as shown in equations (S3.14) and (S3.15).

$X_{N_2} \equiv \frac{F_{N_{2,0}} - F_{N_2}}{F_{N_{2,0}}} = \frac{0.5 F_{NO} + 0.5 F_{NO_2} + F_{N_2O_4}}{F_{N_{2,0}}}$	(S3.10)
$X_{O_2} \equiv \frac{F_{O_{2,0}} - F_{O_2}}{F_{O_{2,0}}} = \frac{0.5 F_{NO} + F_{NO_2} + 2 F_{N_2O_4}}{F_{O_{2,0}}}$	(S3.11)
$X_{N_2} = \frac{F_T (0.5 y_{NO} + 0.5 y_{NO_2} + y_{N_2O_4})}{F_{T0} y_{N_{2,0}}}$	(S3.12)
$X_{O_2} = \frac{F_T (0.5 y_{NO} + y_{NO_2} + 2 y_{N_2O_4})}{F_{T0} y_{O_{2,0}}}$	(S3.13)
$X_{N_2} = \frac{(0.5 y_{NO} + 0.5 y_{NO_2} + y_{N_2O_4})}{0.78 (1 + 0.5 y_{NO_2} + 2 y_{N_2O_4})}$	(S3.14)

$X_{O_2} = \frac{(0.5 y_{NO} + y_{NO_2} + 2 y_{N_2O_4})}{0.21 (1 + 0.5 y_{NO_2} + 2 y_{N_2O_4})}$	(S3.15)
---	---------

#### SI. 4. Derivation of the NO concentration at the GAR's exit

This section presents the derivation that resulted in equation 9 in the main manuscript. The NO concentration at the GAR outlet can only be calculated using a back-calculation approach. A back-calculation approach is the only method by which the NO concentration at the GAR(s) outlet can be calculated. As stated by Tsukahara et al., the NO oxidation presented in equation (S4.1) is a third-order reaction [1]. The post-plasma tubing was considered to be a plug-flow reactor operating at steady state. The corresponding differential equation as a function of post-plasma oxidation time is displayed in equation (S4.2). The rate constant,  $k$  ( $L^2 mol^{-1} s^{-1}$ ), was provided by Tsukahara et al. and is presented in equation (S4.3). As previously outlined in the main manuscript, an isothermal temperature of 20 °C was measured throughout the experiments, and could therefore be treated as a constant. Given the higher oxygen concentration relative to the measured NO concentration, it was assumed that the oxygen concentration remained constant and that the reaction followed pseudo-second-order kinetics. The oxygen volume fraction in the feed was 21%, and its concentration was calculated using the ideal gas law, based on the FTIR inlet temperature and pressure. Separation of independent variables with the appropriate boundary conditions yielded equation (S4.4). Integration resulted in the measured FTIR concentration  $[NO]_t$  after the oxidation time, as displayed in equation (S4.5). Based on rearranging equation (S4.5), the NO concentration at the reactor outlet  $[NO]_{GAR}$  can be calculated, as shown in equation (S4.6).

$2 NO + O_2 \rightarrow 2 NO_2$	(S4.1)
$\frac{d[NO]}{d\tau} = -2k[NO]^2[O_2]$	(S4.2)
$k (L^2 mol^{-1} s^{-1}) = 1.2 \cdot 10^3 \cdot \exp\left(\frac{530}{T(K)}\right)$	(S4.3)
$\int_{[NO]_{GAR}}^{[NO]_t} \frac{1}{[NO]^2} d[NO] = \int_0^{\tau_{oxidation}} -2k[O_2] d\tau$	(S4.4)
$[NO]_t = \frac{[NO]_{GAR}}{2k[NO]_{GAR}[O_2]\tau_{oxidation} + 1}$	(S4.5)
$[NO]_{GAR} = \frac{[NO]}{1 - 2k[NO][O_2]\tau_{oxidation}}$	(S4.6)

- [1] H. Tsukahara, T. Ishida, M. Mayumi, Gas-Phase Oxidation of Nitric Oxide: Chemical Kinetics and Rate Constant, 1999.